Recognition of the 3′ splice site RNA by the U2AF heterodimer involves a dynamic population shift

Lena Voith von Voithenberg[a,b,c,d], Carolina Sánchez-Rico[e,f,g], Hyun-Seo Kang[e,f,g], Tobias Madl[e,f,g,h], Katia Zanier[i], Anders Barth[a,b,c,d], Lisa R. Warner[e,f,g], Michael Sattler[e,f,g,1], and Don C. Lamb[a,b,c,d,1]

[a]Department of Chemistry, Ludwig-Maximilians University, Munich, D-81377 Munich, Germany; [b]NanoSystems Initiative Munich, Ludwig-Maximilians University, Munich, D-81377 Munich, Germany; [c]Center for Integrated Protein Science Munich, Ludwig-Maximilians University, Munich, D-81377 Munich, Germany; [d]Center for Nanoscience, Ludwig-Maximilians University, Munich, D-81377 Munich, Germany; [e]Institute of Structural Biology, Helmholtz Zentrum München, 85764 Neuherberg, Germany; [f]Biomolecular NMR, Technische Universität München, 85748 Garching, Germany; [g]Center for Integrated Protein Science Munich at Fakultät für Chemie, Technische Universität München, 85748 Garching, Germany; [h]Institut für Molekularbiologie und Biochemie, Medizinische Universität Graz, 8010 Graz, Austria; and [i]Biotechnologie et Signalisation Cellulaire, UMR 7242, Ecole Superieure de Biotechnologie de Strasbourg, 67412 Illkirch, France

Edited by Gabriele Varani, University of Washington, Seattle, WA, and accepted by Editorial Board Member Dinshaw J. Patel September 29, 2016 (received for review April 13, 2016)

An essential early step in the assembly of human spliceosomes onto pre-mRNA involves the recognition of regulatory RNA *cis* elements in the 3′ splice site by the U2 auxiliary factor (U2AF). The large (U2AF65) and small (U2AF35) subunits of the U2AF heterodimer contact the polypyrimidine tract (Py-tract) and the AG-dinucleotide, respectively. The tandem RNA recognition motif domains (RRM1,2) of U2AF65 adopt closed/inactive and open/active conformations in the free form and when bound to bona fide Py-tract RNA ligands. To investigate the molecular mechanism and dynamics of 3′ splice site recognition by U2AF65 and the role of U2AF35 in the U2AF heterodimer, we have combined single-pair FRET and NMR experiments. In the absence of RNA, the RRM1,2 domain arrangement is highly dynamic on a submillisecond time scale, switching between closed and open conformations. The addition of Py-tract RNA ligands with increasing binding affinity (strength) gradually shifts the equilibrium toward an open conformation. Notably, the protein–RNA complex is rigid in the presence of a strong Py-tract but exhibits internal motion with weak Py-tracts. Surprisingly, the presence of U2AF35, whose UHM domain interacts with U2AF65 RRM1, increases the population of the open arrangement of U2AF65 RRM1,2 in the absence and presence of a weak Py-tract. These data indicate that the U2AF heterodimer promotes spliceosome assembly by a dynamic population shift toward the open conformation of U2AF65 to facilitate the recognition of weak Py-tracts at the 3′ splice site. The structure and RNA binding of the heterodimer was unaffected by cancer-linked myelodysplastic syndrome mutants.

U2AF | dynamics | splicing | spFRET | NMR

During gene expression, the removal of introns is essential for translation of mature mRNA. The splicing process involves a large number of splicing factors for the correct recognition of introns (1). Whereas U1 snRNP contacts the 5′ splice site, recognition of the 3′ splice site involves binding of SF1/BBP to the branch point sequence (BPS) (2–5) and binding of the U2 auxiliary factor (U2AF) heterodimer to the poly-pyrimidine-tract (Py-tract) that precedes the AG dinucleotide at the intron/exon junction. Binding of U2AF to the 3′ splice site during the early steps of spliceosome assembly recruits the U2 snRNP (6–9). The strength, i.e., splicing efficiency, of a 3′ splice site requires recognition of the BPS, Py-tract, and the AG dinucleotide. However, of these three RNA elements, the Py-tract exhibits the largest degree of variability, and thus, weak to strong splice sites are primarily classified depending on the composition of the Py-tract (7, 10).

U2AF is a heterodimer consisting of a large (U2AF65) and a small (U2AF35) subunit. U2AF65 harbors two canonical RNA recognition motifs (RRM1,2) and an atypical C-terminal RRM domain, called the U2AF homology motif (UHM). U2AF35 has one RRM (which acts as an UHM), flanked N- and C-terminally by two CCCH-type zinc finger motifs, respectively (Fig. S1*A*) (9, 11, 12). The U2AF heterodimer is formed by recognition of a peptide motif, called the UHM Ligand Motif (ULM), in U2AF65 by the U2AF35 UHM domain (13, 14) and enhances RNA binding (15, 16). Recognition of the conserved AG dinucleotide at the 3′ splice site requires U2AF35 (15, 17–20). U2AF65 binds to the Py-tract sequence located at the 3′ splice site via its RRM domains. The Py-tract sequence is degenerate in eukaryotes (21, 22), and the efficiency of the 3′ splice site recognition largely depends on the Py-tract strength, i.e., the number of uridines present in the sequence (8, 9). U2AF65 is sufficient for splicing of introns harboring strong Py-tracts in vitro, whereas U2AF35 is required for splicing of introns with weak (low-affinity) Py-tracts and is essential in vivo (7, 10, 23–25). The substantial variability in Py-tracts and plasticity in intron recognition is exploited for alternative splicing, which in eukaryotes occurs in over 60% and in humans in the majority of multiexon genes (21, 26, 27).

Recently, it was proposed that Py-tract RNA binding by U2AF65 employs a conformational selection mechanism, which involves a population shift of the arrangement of its tandem RRM domains from a closed to an open state (28). Moreover, based on a combined analysis of NMR and small angle X-ray scattering (SAXS) data, it has been shown that the unbound RRM1,2 protein adopts a range of closed and detached domain arrangements, which are not able to mediate high-affinity RNA binding (29). To understand the

Significance

The splicing of human pre-mRNAs is tightly controlled and regulated during the assembly of the spliceosome onto pre-mRNA introns. Recognition of regulatory RNA sequence motifs by splicing factors is an essential early step during spliceosome assembly. We combine single-pair FRET and NMR to show that the recognition of the 3′ splice site in pre-mRNA introns by the essential heterodimeric splicing factor U2 auxiliary factor (U2AF) involves conformational dynamics and population shifts of its RNA binding domains between open and closed conformations. Unexpectedly, the small subunit U2AF35 facilitates the recognition of weak splice sites by a population shift of the RNA binding domains of U2AF65 toward the open conformation. Notably, disease-linked mutations in U2AF65 do not affect RNA or U2AF35 binding.

Author contributions: L.V.v.V., C.S.-R., H.-S.K., T.M., K.Z., L.R.W., M.S., and D.C.L. designed research; L.V.v.V., C.S.-R., H.-S.K., T.M., and K.Z. performed research; A.B. contributed new reagents/analytic tools; L.V.v.V., C.S.-R., H.-S.K., T.M., and K.Z. analyzed data; and L.V.v.V., C.S.-R., H.-S.K., M.S., and D.C.L. wrote the paper.

The authors declare no conflict of interest.

This article is a PNAS Direct Submission. G.V. is a Guest Editor invited by the Editorial Board.

[1]To whom correspondence may be addressed. Email: d.lamb@lmu.de or sattler@helmholtz-muenchen.de.

This article contains supporting information online at www.pnas.org/lookup/suppl/doi:10.1073/pnas.1605873113/-/DCSupplemental.

molecular mechanisms of these conformational changes and characterize the underlying conformational dynamics induced by RNA binding, we applied single-pair Förster resonance energy transfer (spFRET). The detailed investigation of the conformational dynamics on the single-molecule level revealed that the arrangement of the U2AF65 RRM1,2 tandem domains switches between an open and closed conformation. Increasing binding affinity to Py-tract RNA ligands correlates with a population shift toward the open state. Only strong Py-tracts promote the formation of a rigid protein–RNA complex, whereas complexes with weaker, i.e., lower-affinity, RNA ligands, still show significant conformational dynamics. Most notably, the presence of the small subunit, U2AF35, shifts the U2AF65 RRM1,2 domain arrangement toward an open, active conformation already in the absence of RNA, consistent with the known requirement of U2AF35 to enhance the recognition of weak Py-tracts by U2AF.

Results

The RRM1,2 Domains of U2AF65 Are Highly Dynamic. The two RNA recognition motifs 1 and 2 (RRM1,2), connected by a flexible linker, represent the minimal RNA binding region for U2AF65 (Fig. S1) (8, 28, 30). Molecular details of the RNA recognition of the individual RRM1 and RRM2 domains have been described previously (30). Recently, it was shown that U2AF65 RRM1,2 exists in a closed conformation in its free form and an open conformation when RNA is bound (28). An enhancement of the overall RNA binding affinity with increasing Py-tract strength correlates with a population shift toward the open conformation. NMR data demonstrate that this shift involves an increased contribution of RRM1 to RNA binding (28). To investigate the role of conformational dynamics in this population shift, we used spFRET to study the intrinsic dynamics of RRM1,2 in the absence and presence of RNA. For these experiments, one residue in each of the RNA recognition motifs RRM1 and RRM2 was mutated to a cysteine residue and labeled stochastically with a donor and acceptor dye pair (Fig. 1*A* and Fig. S1*C*). The cysteine positions were designed to be in close proximity when the RRM1,2 tandem domains adopt a closed conformation and to be at maximal distance when the domains adopt an open conformation (28). To ensure that the measurements are not subject to artifacts from the labeling, we analyzed the FRET efficiency and conformational change of the protein using different fluorescent labels and tested different labeling positions (Figs. S2 and S3). The constructs were measured in solution using a confocal microscope with multiparameter fluorescence detection and pulsed interleaved excitation (MFD-PIE) (31–34).

In the spFRET efficiency histogram, the free form of RRM1,2 is found to populate a high FRET state with a mean FRET efficiency of 0.78 (Figs. 1*B* and 2*A* and Table S1). By analyzing the lifetime information of the donor fluorophore, we could determine that this FRET efficiency is an average value obtained from a highly dynamic population of molecules (Fig. 1*B*, *Left*). In burst analysis experiments, an average FRET efficiency and donor lifetime is determined for each molecule. When molecules undergo conformational dynamics during their transit time through the confocal volume (of a few milliseconds), an average single-molecule FRET efficiency is measured. The presence of dynamics on the submillisecond time scale can be visualized by plotting the intensity-determined FRET efficiency versus donor lifetime. In the presence of dynamics, the intensity-determined FRET efficiency will be a species-averaged value (Eq. **S6**), whereas the donor lifetime is a lifetime-weighted average (Eq. **S7**). This yields a deviation from the relationship observed for a static FRET species (static FRET line; Eq. **S5**) (32, 35, 36). In Fig. 1*B*, *Left*, all molecules clearly deviate from the static FRET line, demonstrating that the conformation of RRM1,2 is highly dynamic in the absence of RNA. By combining the lifetime information for all the single-molecule in the spFRET experiments, we observed two donor lifetimes of 0.14 and 2.15 ns for

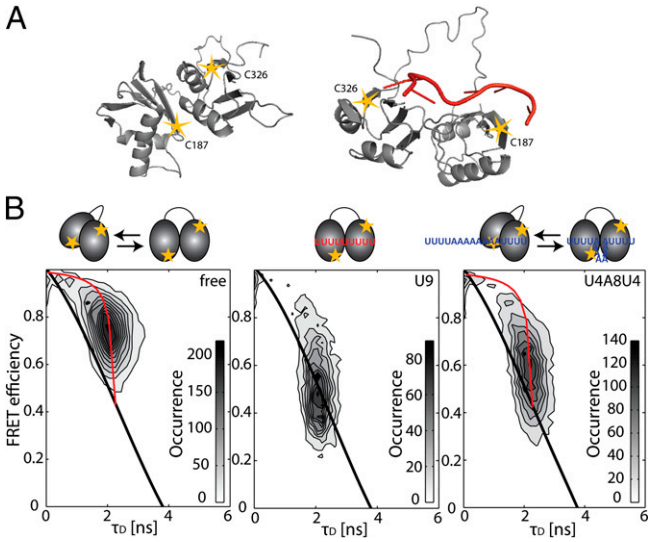

Fig. 1. Conformation and dynamics of RRM1,2 in solution. (*A*) Closed (*Left*, PDB 2YH0) and open, RNA-bound (*Right*, PDB 2YH1) structure of U2AF65 (RRM1,2) with labeling sites C187 in RRM1 and C326 in RRM2 shown as stars. (*B*) Histogram of spFRET efficiency as a function of donor lifetime of RRM1,2-Atto532-Alexa647 in the absence of RNA (9,160 molecules), in the presence of 5 μM U9 (10,015 molecules), or in the presence of 20 μM U4A8U4-RNA (12,083 molecules). Populations of static molecules are described by the polynomial static FRET line (Eq. **S5**; black line), whereas molecules undergoing conformational dynamics on the time scale of microseconds to milliseconds deviate from this line (dynamic FRET curve in Eq. **S7**; red line). The fully open and closed conformations were determined from lifetime fits of the data and correspond to the intersections of the dynamic FRET curve with the static FRET line (Fig. S2*B*). Representations of the open and closed conformations of the molecules are displayed schematically as a simple interpretation of the histograms.

the free form of RRM1,2, corresponding to FRET efficiencies of 0.96 and 0.43, respectively (Table S1, Fig. 1*B*, and Fig. S2*B*). Thus, we conclude that the protein undergoes conformational transitions between a closed conformation, an arrangement of the tandem domains where the donor–acceptor separation is ∼34–40 Å and an open conformation with a distance of 64–69 Å. Estimations of the spFRET histograms for the open and closed conformation are shown in Fig. 2*D*. Using accessible volume calculations (35), we estimated the average donor–acceptor separation from the published structures of 42 Å for the closed conformation (PDB 2YH0) (28) and a distance of 61 Å for the open conformation (PDB 2YH1). The measured FRET distances and accessible volume calculations are in excellent agreement, especially when considering that the tandem RRMs represent an ensemble of closed and detached conformations with respect to each other as indicated from the NMR and SAXS data (29).

From the mean FRET efficiency and the FRET values obtained for the open and closed states from the donor lifetime data, we could estimate the fraction of time each molecule spends in the open conformation (Table S1). Free RRM1,2 molecules mainly populate the closed high FRET state (with a donor–acceptor separation of ∼35 Å) spending an average of just ∼1/3 of their time in the open conformation with a distance of ∼65 Å between the fluorophores.

A linker truncation mutant RRM1,2-Δ233–252, which was previously proposed to increase the population of the open domain arrangement (28), was investigated. This construct adopts a closed conformation with the same FRET efficiency as observed for RRM1,2, whereas the open conformation exhibits a slightly higher FRET efficiency (*SI Text* and Fig. S3*B*). Thus, truncation of the inner part of the linker region does not abolish the conformational dynamics of the unbound RRM1,2, whereas it promotes an open conformation that is not as extended as in the wild-type protein. At the same time, the mutant serves as an internal control

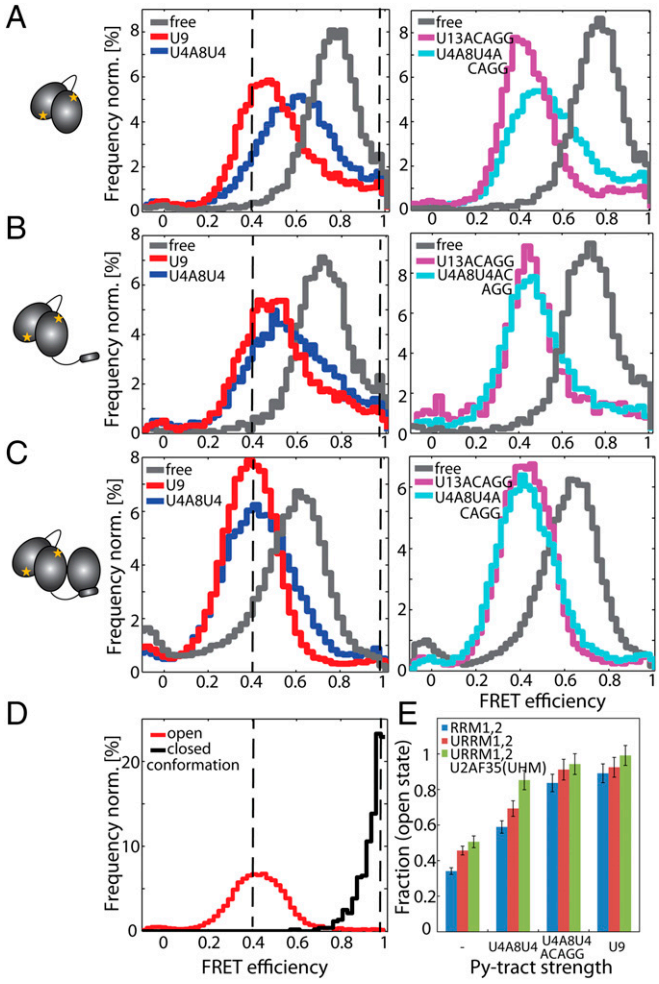

Fig. 2. Comparison of the conformations of the U2AF65-C187-C326 constructs RRM1,2, URRM1,2, and URRM1,2/U2AF35(UHM). SpFRET experiments of the constructs were performed in solution using MFD-PIE. Schematic representations of the minimal (*A*) RRM1,2, (*B*) URRM1,2, and (*C*) URRM1,2/U2AF35(UHM) are shown on the left. SpFRET efficiency histograms of RRM1,2 (*A*), URRM1,2 (*B*), and URRM1,2/U2AF35(UHM) (*C*) are displayed in the free form (gray) or in the presence of U9 (red), U4A8U4 (blue), U13ACAGG (pink), and U4A8U4ACAGG (cyan). The dashed black lines serve as guides to the eye to show the peak FRET efficiency for the open and closed conformations as obtained from *D*. (*D*) Estimation of the open and the closed state of RRM1,2. The FRET efficiency histogram of RRM1,2 molecules with a donor lifetime $\tau_D < 1$ ns (black) was selected to represent the closed conformation. The FRET efficiency histogram of U13ACAGG-bound URRM1,2/U2AF35(UHM) with a donor lifetime $\tau_D > 1$ ns (red) was selected to represent the open conformation. (*E*) Quantitative description of the dynamic equilibrium in a bar diagram displaying the fraction of time the different U2AF65 constructs spend in the open conformation based on the spFRET experiments of the constructs in solution (RRM1,2, blue; URRM1,2, red; URRM1,2/U2AF35(UHM), green). Errors were determined by error propagation from the values of E_1, E_2, and $\langle E \rangle$ (Table S1).

to show that another different open conformation can be adopted and recognized by the lifetime analysis and supports that observation that the open conformation observed for all full-linker constructs in the absence and presence of RNA is the same.

U2AF65 Adopts an Open State When Binding to Strong Py-Tracts. Next, we analyzed the conformational states of the minimal RRM1,2 in the presence of RNA substrates. For the strong Py-tract (U9), the apparent FRET efficiency shifts to an average value of around 0.5 (Fig. 1*B* and Table S1). The spFRET histogram represents a mixture of the same open and closed conformations as observed for the free protein (FRET efficiencies 0.97 and 0.44 for U9-bound RRM1,2) (Table S1). However, the equilibrium between the open and closed conformation of RRM1,2 is shifted significantly, with the complex spending around 90% of the time in the open conformation (Figs. 1*B*, *Middle*, and 2*A*). The population clearly lies on the static FRET curve indicating a stabilization of the open conformation. For a weaker Py-tract (U4A8U4), the apparent average FRET efficiency is 0.63 and the population deviates from the static FRET line (Figs. 1*B*, *Right*, and 2*A*). This indicates an increase in dynamics compared with the U9-bound U2AF65. Again, the spFRET data and fluorescence lifetime data reveal dynamic transitions between two states with FRET efficiencies of 0.40 ($D = 66$ Å) and 0.97 ($D = 35$ Å), i.e., the same two populations observed previously. The molecules populate the open conformation 59% of the time, whereas they were still found in the closed conformation quite frequently. Hence, the equilibrium between the open and the closed conformation of U2AF65 is influenced by the overall binding affinity for the Py-tract sequence. Py-tracts with higher affinity lead to a shift in the equilibrium by increasing the time the molecules spend in the open conformation. Consistently, purine-rich RNA ligands such as A9 and A13ACAGG that do not contain bona fide Py-tract sequences do not induce any shift in the FRET efficiency histogram or influence the conformational dynamics of RRM1,2 constructs with respect to the same protein in the absence of RNA (Fig. S2 *E* and *F*).

We investigated whether additional conformational changes are observable on a slower time scale with spFRET–total internal reflection fluorescence microscopy. Static RRM1,2-C187-C318-Atto532/Alexa647 molecules with FRET efficiencies corresponding to the conformations observed in solution-based measurements but no evidence for conformational transitions on time scales longer than 30 ms were found (Figs. S3 and S4).

Role of U2AF35 for Py-Tract Recognition by the U2AF Heterodimer. The ULM region of U2AF65 is necessary for binding to the U2AF35 subunit and thus formation of the U2AF heterodimer. Hence, before studying the conformation of U2AF65 in the presence of U2AF35, we first characterized an extended U2AF65 RRM1,2 protein that includes the ULM region (URRM1,2) in the absence and presence of RNA (Fig. 2*B* and Figs. S3*C* and S5*B*). We found a similar behavior as was observed for RRM1,2 without the additional ULM region. Dynamic transitions between the open and closed conformations were observed with the same FRET efficiencies of 0.44 and 0.95 as was observed for RRM1,2 alone. We observed an overall shift of the equilibrium toward the open conformation with URRM1,2 spending 46% of the time in the open conformation in the absence of RNA (compared with 34% for RRM1,2) (Fig. 2 *A* and *B* and Table S1). Binding of the strong Py-tract U9 and the weak Py-tract U4A8U4 to URRM1,2 induced a shift of the equilibrium toward the open state with the molecules now spending 92% and 69% of their time in the open conformation, respectively (Table S1). Isothermal titration experiments show that the addition of amino acids 88–147, preceding the RRM1 domain, increases the affinity of URRM1,2 sixfold compared with RRM1,2 alone (Table S2). We could show that this increased affinity is associated with faster binding rates (Table S2). An increasingly open conformation is thus accompanied by an increase in the binding kinetics.

Next, we investigated the role of U2AF35 in Py-tract recognition at the 3′ splice site. The U2AF35 UHM domain mediates protein–protein interactions (13, 14) and folds upon binding to a UHM Ligand Motif (ULM) peptide sequence in U2AF65 (11) but does not directly contribute to the specific recognition of the AG-dinucleotide by U2AF35 (37). Instead, two conserved zinc finger domains flanking the UHM are expected to mediate the specific recognition at the 3′ splice site (20). To understand the contribution of the U2AF35 UHM domain to Py-tract recognition by U2AF65, we studied the RRM1,2 domain arrangements

in the context of a minimal U2AF heterodimer, which has been used in previous studies (17, 19). The minimal U2AF heterodimer comprises the U2AF65 ULM and the RRM1,2 domains bound to the U2AF35 UHM domain (URRM1,2/U2AF35(UHM)). We measured the conformation of the RRM1,2 domains within the minimal heterodimer in the absence and presence of RNA. As before, we observed dynamics between the same open and closed conformations with the heterodimer spending even more time in the open conformation (51%) with respect to RRM1,2 (34%) and URRM1,2 (46%) (Table S1). Correspondingly, the affinity of the URRM1,2/U2AF35(UHM) heterodimer (K_D = 150 nM) for the strong Py-tract U9 is higher than for RRM1,2 (K_D = 1.34 μM) and URRM1,2 (K_D = 220 nM) (Table S2). The shift of the equilibrium in the presence of U2AF35(UHM) is more strongly pronounced in the presence of weak Py-tract RNA, 99% in the open conformation for the strong U9 Py-tract versus 90% without U2AF35 and 85% for the weaker ligand (U4A8U4) versus 59% when the small subunit is absent (Table S1). The presence of U2AF35 has a large effect in shifting RRM1,2 to the open conformation when the weak Py track is bound (U4A8U4). U2AF35 also shifts RRM1,2 more to the open state when a strong Py-tract is bound, but this effect is less dramatic because the complex already exists predominantly in the open conformation. In either case, the likelihood of the heterodimer to be found in the open state is significantly increased compared with RRM1,2 or URRM1,2.

To explore potential contributions of additional RNA sequences present in the 3′ splice site on the RRM1,2 conformational equilibrium, we studied the interaction with an RNA comprising a strong Py-tract followed by an AG splice site, U13ACAGG. U2AF65 RRM1,2 shows the same open and closed conformations as in the presence of the shorter Py-tract U9 (Fig. 2*A*), consistent with the expectation that RRM1,2 specifically recognizes the Py-tract region of the RNA. The RRM1,2 proteins spend around 96% of the time in the open conformation. Upon binding to a weak Py-tract followed by the AG splice site, U4A8U4ACAGG, the equilibrium is shifted toward the open state (84%) compared with the binding of the weak Py-tract without the extended AG sequence, U4A8U4 (59%) (Fig. 2*A* and Table S1). Presumably, additional, nonspecific contacts involving the additional nucleotides following the weak Py-tract can induce a population shift toward the open state.

We also observe an increased stabilization of the open conformation upon binding of a weak Py-tract to URRM1,2 (Fig. 2*B* and Fig. S3*C* and Table S1). In the presence of U4A8U4ACAGG, URRM1,2 proteins spend 91% of their time in the open conformation compared with 69% for U4A8U4. This may correlate with the higher overall binding affinity of URRM1,2 for U4A8U4ACAGG than for U4A8U4. Additional contacts between U2AF65 and the additional nucleotides present downstream of the Py-tract thus lead to a higher probability of the RRM domains to be found in the open conformation. Additional chemical shift perturbations in the NMR data also revealed stabilizing RNA contacts for a few residues preceding the first β1-strand in RRM1 (Fig. S6*A*), consistent with a recent crystal structure of an extended RRM1,2 protein bound to a strong Py-tract (38). However, the NMR titration data also demonstrate that no additional contacts are observed for residues preceding this N-terminal region of RRM1.

U2AF35 Enhances Py-Tract Recognition by a Dynamic Population Shift. Surprisingly, in the minimal heterodimer, the population of the open conformation of RRM1,2 is substantially increased even in the absence of RNA, going from 34% for RRM1,2 and 46% for URRM1,2 to 51% in the U2AF heterodimer (Fig. 2 and Fig. S3 *C* and *D*). This indicates that the presence of the U2AF35 UHM domain enhances the open conformation of U2AF65 RRM1,2. Consistent with the increased fraction of open conformations in the unbound U2AF heterodimer, binding of a weak Py-tract U4A8U4ACAGG shows a dramatic population shift toward the open conformation similar to that measured in the presence of U9 (94% for U4A8U4ACAGG versus 99% for U9) (Fig. 2*C* and Table S1). A control experiment of RRM1,2 without the ULM binding domain in the presence of U2AF35(UHM) and U4A8U4ACAGG could not induce this stabilization of the open conformation (Fig. S5*A*). Thus, the presence of the U2AF35 UHM domain, when stably bound in the U2AF heterodimer, leads to a population shift of the RRM1,2 domains toward the open conformation. Thereby, the heterodimer promotes an open conformation that enables efficient binding even of weak Py-tract RNA ligands (Table S1 and Fig. 2 *C* and *E*).

An Interface in the U2AF Heterodimer Mediates the Population Shift. To characterize the structural mechanisms of how U2AF35 leads to a population shift toward the open conformation of RRM1,2, we studied the domain arrangements in the minimal U2AF heterodimer [URRM1,2/U2AF35(UHM)] using NMR spectroscopy. We determined local tumbling correlation times from ^{15}N NMR relaxation data for the free U2AF heterodimer and when bound to a strong Py-tract AG RNA (U13ACAGG). These data indicate that, in the absence of RNA, the U2AF65 ULM, RRM1, and the U2AF35 UHM domains tumble together, whereas the U2AF65 RRM2 domain exhibits higher mobility (Fig. 3*A*). This suggests that the RRM2 may be partially detached from RRM1. In contrast, upon formation of the U2AF/RNA complex, all domains in both subunits tumble together, indicating the formation of a compact and rigid protein/RNA complex (Fig. 3 *B* and *C*).

The relative arrangement of the domains in the U2AF heterodimer/RNA complex was determined by paramagnetic relaxation enhancement (PRE) data with single nitroxyl spin labels attached to specific sites in U2AF65 RRM1, RRM2, and U2AF35 UHM (Fig. 3 *D* and *F* and Fig. S6). Notably, SL155 shows the same PRE effects for RRM1,2 in the context of the heterodimer bound to the extended strong Py-tract as observed for RRM1,2 alone bound to a strong Py-tract (Fig. S6*C*). This is fully consistent with the FRET data, which indicate that the same open conformation is adopted upon binding to strong Py-tracts. A number of spin labels attached to RRM1 or UHM show strong intermolecular PRE effects between these two domains (Fig. 3 and Fig. S6). These data demonstrate that the U2AF35 UHM domain shares a binding interface with the U2AF65 RRM1 domain in addition to the known recognition of the U2AF65 ULM peptide on the helical face of the UHM domain. A structural model for the domain arrangements in the U2AF heterodimer when bound to a strong 3′ splice site Py-tract AG RNA is shown in Fig. 3*F*. Notably, the same interaction is already present in the absence of RNA (Fig. S6*D*). Thus, the RRM1/UHM domain interaction destabilizes the closed conformation of the U2AF65 RRM1,2 tandem domains and thereby promotes the population shift toward the open domain arrangement and thus contributes to an increased RNA affinity even for weak Py-tracts.

Disease-Linked Mutations in U2AF65 Do Not Affect the Structure and RNA Binding of the U2AF Heterodimer. Yoshida et al. (39) described point mutations in several components of the splicing machinery leading to myelodysplastic syndromes. Here we investigated the effect of the confirmed somatic mutations L187V and M144I. To analyze whether these mutations could affect the structure of U2AF65 or the conformation of the heterodimer [by modulating the interface with U2AF35(UHM)], we compared NMR spectra of ^{15}N-labeled U2AF65 in the wild-type heterodimer with URRM1,2-M144I/U2AF35(UHM) and URRM1,2-L187V/U2AF35(UHM). Analysis of the chemical shift differences shows mainly local effects in the vicinity of the mutation (Fig. 4). This demonstrates that the structure of U2AF65 RRM1,2 and the formation of the U2AF heterodimer is not affected by these disease mutations. We then tested if the mutations could affect RNA binding by the

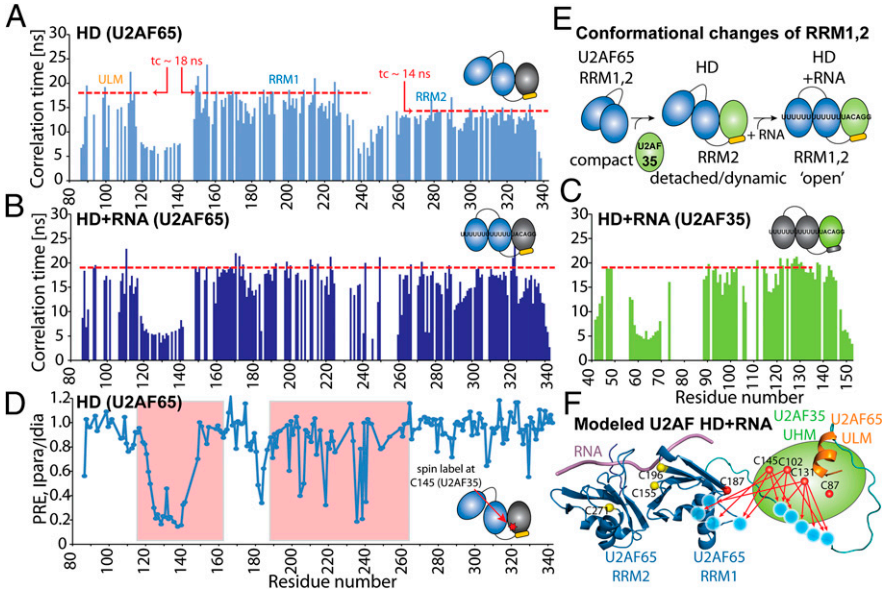

Fig. 3. NMR ^{15}N-relaxation–based rotational correlation time of the U2AF heterodimer in the (*A*) absence and (*B* and *C*) presence of U13ACAGG (*B*) for URRM1,2 and (*C*) for U2AF35(UHM). Conformational changes of the domains in the U2AF heterodimer URRM1,2/U2AF35(UHM) upon binding of U2AF35 (UHM) and RNA are shown as schematic diagrams. Two distinct rotational correlation times are shown in *A*. Missing data points denote proline, unassigned, or spectrally overlapped residues. (*D*) PREs (ratio of NMR signal intensities in the paramagnetic and diamagnetic state, I_{para}/I_{dia}) observed in URRM1,2 (red box) upon binding of U2AF65(UHM) (spin labeled at C145). (*E*) Stepwise schematic diagram depicting conformational changes of RRM1,2 and U2AF65/35 interfaces by introducing U2AF35(UHM), followed by RNA addition. (*F*) PRE-based model of the U2AF heterodimer URRM1,2/U2AF35(UHM) in the presence of RNA, with spin labels attached to multiple sites in U2AF to define the relative orientations/conformations of RRM1,2 (yellow circle) and U2AF65/35 (red circle). Selected key regions with intersubunit PREs in U2AF65/35 are highlighted (cyan circles) and connected to the corresponding spin label sites (red arrow).

U2AF heterodimer by using isothermal titration calorimetry (ITC) (Fig. S7 *A* and *B*) and fluorescence correlation spectroscopy (FCS) (Fig. S7 *C* and *D*). We measured the binding affinities of both mutants for the strong and weak Py-tract RNAs and compared them to the wild-type heterodimer (Table S3). All three constructs showed similar RNA binding affinities with an approximately sevenfold higher RNA binding affinity in the presence of U2AF35(UHM). This demonstrates that U2AF35 still contributes to the overall RNA binding in the mutant heterodimers. We did, however, observe a more aggregation-prone behavior of the two point mutants compared with the wild type in FCS experiments. The point mutations in URRM1,2 leading to myelodysplastic syndromes, therefore, do not directly influence the binding affinity of the RNA or binding of the small subunit U2AF35. This suggests that these mutations potentially affect interactions with other factors.

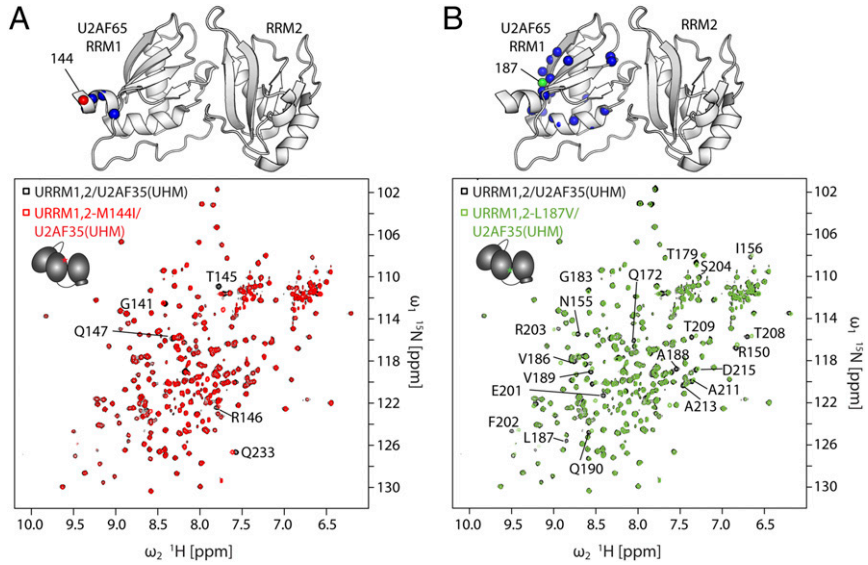

Fig. 4. NMR spectra of U2AF heterodimers formed with U2AF35(UHM) and URRM1,2 harboring the somatic point mutations (*A*) M144I and (*B*) L187V. (*Top*) Notable chemical shift changes for amides in U2AF65 observed for the heterodimers harboring the mutations are indicated as red spheres on RNA-bound RRM1,2 (PDB 5EV1). (*Bottom*) The ^{1}H,^{15}*N*-HSQC spectra of URRM1,2/U2AF35(UHM) (black), URRM1,2-M144I/U2AF35(UHM) (red), and URRM1,2-L187V/U2AF35 (UHM) (green).

Discussion

RNA binding of U2AF65 is associated with an open domain configuration, whereas unbound U2AF65 represents an ensemble of closed conformations (28, 29). When analyzing its conformational dynamics, we found that U2AF65 can adopt different conformational states, dynamically switching between a closed conformation with a FRET efficiency of ∼0.96 and an open state with a FRET efficiency of ∼0.43. The free form of U2AF65 is highly dynamic on the submillisecond time scale spending ∼1/3 of the time in the open conformation (Fig. 2*E*). This is fully consistent with the NMR spectra, which show a single set of signals, indicating conformational averaging that is fast on the NMR chemical shift time scale (i.e., less than milliseconds). We do not observe conformational dynamics on time scales longer than 30 ms. Agrawal et al. (38) described conformational dynamics of U2AF65 on the time scale of 5–30 s. Although the different types of spFRET measurements reveal different dynamic time scales, they consistently show more dynamics in the absence of RNA, and the open conformation of U2AF65 is stabilized in the presence of a strong Py-tract.

High-affinity Py-tracts strongly stabilize the open, active conformation of the complex. This effect is reduced for weak Py-tract sequences. We found a correlation between the dynamic equilibrium between the open and closed conformation and the binding affinity of the complexes (Fig. 2*E*). An increase in the population of the open state corresponds to a higher probability for prespliceosomal complex formation (28) because the open conformation is the active form of U2AF65 required for spliceosome assembly.

Alternative splicing occurs in 90% of all human genes and is extremely important for the high level of phenotypic complexity in mammals (26, 27). Py-tracts of higher eukaryotes contain only 50% uridines, whereas 30% of the nucleotides are cytosines and 10% adenines and guanines, each (40). Moreover, although the binding site in U2AF65 and the consensus length of Py-tracts corresponds to eight pyrimidines (28), Py-tracts found in natural 3′ splice site sequences can span 30 or more nucleotides. U2AF65 therefore has to be able to recognize a variety of Py-tract sequences and lengths (6), while at the same time being able to specifically and unambiguously identify bona fide splice sites. The splicing efficiency depends proportionally on the number of consecutive uridines in the sequence (7, 22). We observed a similar trend when analyzing the dynamics of U2AF65 between its open and its closed conformation. The equilibrium of U2AF65 shifts toward the open conformation with increasing Py-tract strength. The presence of additional residues flanking RRM1 in URRM1,2 and the binding of U2AF35 also shift the equilibrium of the complex toward the open conformation (Fig. 2*E*). The additional amino acids present in URRM1,2 compared with RRM1,2 enhance the RNA binding affinity (Table S2), consistent with a recent study that indicates that N- and C-terminally flanked regions in U2AF65 RRM1,2 mediate additional RNA contacts (38).

An important finding of our study is that the open conformation is further stabilized by binding of the small subunit U2AF35 (Fig. 2*E*). Our NMR data show that this involves an interaction between the U2AF35 UHM domain and U2AF65 RRM1 (Fig. 3). The shift in equilibrium is already induced in the absence of RNA and thus greatly enhances the overall affinity for weak Py-tracts. This is consistent with the requirement of U2AF35 for splicing of introns with weak 3′ splice sites and for viability in eukaryotes (18, 41, 42), whereas AG-independent introns exhibit strong Py-tract sequences, for which U2AF35 is not necessarily required (7, 23, 25). However, the molecular details for the recognition of weak 3′ splice sites remain poorly understood. Recent reports indicate that the zinc fingers flanking the U2AF35(UHM) domain mediate direct recognition of the 3′ splice site AG dinucleotide (20), consistent with the fact that the U2AF35(UHM) does not contribute to RNA binding in the context of a minimal heterodimer [U2AF65(RRM1,2)/U2AF35(UHM)] lacking the zinc finger domains (37). Nevertheless, our data demonstrate that the small subunit U2AF35(UHM) allosterically enhances the interaction of U2AF65 with weak Py-tract RNA sequences by inducing a population shift toward the open conformation already in the absence of RNA. This unexpected finding also implies an indirect role for the UHM domain for 3′ splice site recognition, which will enhance the recognition of weak Py-tracts by stabilization the open conformation of U2AF65 RRM1,2 (Fig. 5).

It is important to note that the population shifts involving the RNA binding domains of U2AF for 3′ splice site recognition are not affected by the presence of SF1 and its binding to the BPS sequence. Comparison of NMR spectra of U2AF65, the U2AF heterodimer, and U2AF65-SF1 complexes demonstrates that the conformations and conformational arrangements coupled with RNA binding of U2AF are not affected by the presence of SF1 (43, 44). Thus, although 3′ splice site recognition involves cooperative binding of SF1, U2AF65, and U2AF35, the fine-tuning and regulation of the assembly depends on the variability in the Py-tract and its recognition by population shifts involving the RNA binding domains of the U2AF heterodimer. It will be interesting to analyze how additional factors, such as hnRNP A1 (45) or phosphorylation of SF1 (44, 46, 47), influence 3′ splice recognition by U2AF.

In summary, we provide insight into the underlying molecular mechanism of U2AF binding to 3′ splice sites. An emerging paradigm resulting from the current and our previous study (28) is that the high splicing efficiency is introduced by a stabilization of the open conformation of U2AF65. Because the open conformation is significantly populated already in the absence of RNA, protein–RNA complex formation uses a conformational selection mechanism. Py-tracts with varying strength correlate with splicing efficiencies and are reflected in the equilibrium between the two conformational states (this work and ref. 28). Nevertheless, depending on the Py-tract strength, an initial RNA binding to RRM2 in the closed state with a subsequent conformational change may contribute to complex formation. This would allow fly-casting of the RRM1 domain to scan the RNA and identify Py-tracts in the context of introns with extended Py-tract regions (28). Most importantly, our data imply that the population shift induced by the U2AF35 UHM domain, combined with direct recognition of the AG-dinucleotide by the U2AF35 zinc fingers, contributes to the fidelity of 3′ splice site recognition by U2AF as an essential early step in spliceosome assembly.

Methods

Plasmids and Constructs. The human RRM1,2 (U2AF65-148-342) minimal RNA binding mutant, RRM1,2-Δ233–252, URRM1,2 (U2AF65-88-342), and U2AF35(UHM) [U2AF35(38-152)] were cloned by PCR amplification (Fig. S1*A*). The constructs were inserted into a pETM11 (U2AF65) or pET9d (U2AF35) vector containing an N-terminal 6xHis-tag (28). Double cysteines were introduced into U2AF65 constructs by site-directed mutagenesis at positions C187/C318 or C187/C326.

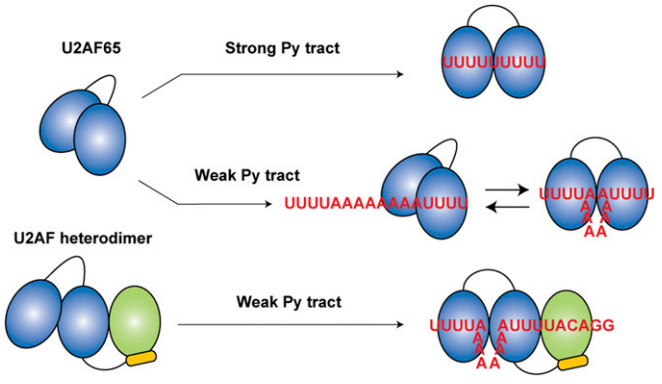

Fig. 5. Summary of the conformational changes observed in U2AF65 RRM1,2 and the U2AF heterodimer upon binding to strong and weak Py-tract RNAs.

Expression and Purification of Recombinant Proteins. U2AF65 mutants were expressed in *Escherichia coli* BL21(DE3) and purified as described in Mackereth et al. (28). For the U2AF heterodimer, URRM1,2 and U2AF35(38-152) were expressed and purified separately, incubated at equimolar ratios, and purified as a complex by size-exclusion chromatography as described in Kellenberger et al. (11).

Single-Pair FRET Measurements. Single-pair FRET measurements were performed on a custom-build confocal microscope using multiparameter fluorescence detection with pulsed interleaved excitation (*SI Text*) (32). Proteins were site-specifically labeled at cysteines and diluted to concentrations of 20–50 pM in 20 mM potassium phosphate (pH 6.5), 50 mM NaCl. Measurements were performed with proteins in their free form or mixed with 5 μM of U9, U13ACAGG, A9, or A13ACAGG or 20 μM of U4A8U4, U4A8U4ACAGG, or U4A8U5ACAGG.

NMR Spectroscopy. All NMR samples contained protein concentrations of 0.1–0.5 mM in 20 mM sodium phosphate (pH 6.5), 50 mM NaCl, 2 mM DTT, and 5–10% (vol/vol) ^2H_2O. Spectra were recorded at 295 K and analyzed using Sparky 3 in combination with previously published assignments (28).

ACKNOWLEDGMENTS. We thank W. Kügel for providing the burst analysis software, and W. Schrimpf and J. Valcarcel for valuable discussions. We are grateful to Y. Zhang for constructs used in preliminary experiments and G. Demiraslan for technical assistance. We gratefully acknowledge the financial support of the Deutsche Forschungsgemeinschaft through Grants SFB1035 (Projects A11, B03) and GRK1721, and support from the Ludwig-Maximilians-Universität through the Center for NanoScience and the BioImaging Network. T.M. was supported by the Bavarian Ministry of Sciences, Research and the Arts (Bavarian Molecular Biosystems Research Network), the German Research Foundation (Emmy Noether Program MA 5703/1-1), and the Austrian Science Fund (FWF; Grants P28854 and DK-MCD W1226). L.R.W. acknowledges a Long-Term EMBO postdoctoral fellowship (Grant ALTF 1520-2011).

1. Will CL, Lührmann R (2011) Spliceosome structure and function. *Cold Spring Harb Perspect Biol* 3(7):a003707.
2. Berglund JA, Abovich N, Rosbash M (1998) A cooperative interaction between U2AF65 and mBBP/SF1 facilitates branchpoint region recognition. *Genes Dev* 12(6):858–867.
3. Berglund JA, Chua K, Abovich N, Reed R, Rosbash M (1997) The splicing factor BBP interacts specifically with the pre-mRNA branchpoint sequence UACUAAC. *Cell* 89(5):781–787.
4. Liu Z, et al. (2001) Structural basis for recognition of the intron branch site RNA by splicing factor 1. *Science* 294(5544):1098–1102.
5. Rain JC, Rafi Z, Rhani Z, Legrain P, Krämer A (1998) Conservation of functional domains involved in RNA binding and protein-protein interactions in human and Saccharomyces cerevisiae pre-mRNA splicing factor SF1. *RNA* 4(5):551–565.
6. Banerjee H, Rahn A, Davis W, Singh R (2003) Sex lethal and U2 small nuclear ribonucleoprotein auxiliary factor (U2AF65) recognize polypyrimidine tracts using multiple modes of binding. *RNA* 9(1):88–99.
7. Reed R (1989) The organization of 3′ splice-site sequences in mammalian introns. *Genes Dev* 3(12B):2113–2123.
8. Singh R, Valcárcel J, Green MR (1995) Distinct binding specificities and functions of higher eukaryotic polypyrimidine tract-binding proteins. *Science* 268(5214):1173–1176.
9. Zamore PD, Patton JG, Green MR (1992) Cloning and domain structure of the mammalian splicing factor U2AF. *Nature* 355(6361):609–614.
10. Moore MJ (2000) Intron recognition comes of AGe. *Nat Struct Biol* 7(1):14–16.
11. Kellenberger E, Stier G, Sattler M (2002) Induced folding of the U2AF35 RRM upon binding to U2AF65. *FEBS Lett* 528(1-3):171–176.
12. Mollet I, Barbosa-Morais NL, Andrade J, Carmo-Fonseca M (2006) Diversity of human U2AF splicing factors. *FEBS J* 273(21):4807–4816.
13. Kielkopf CL, Rodionova NA, Green MR, Burley SK (2001) A novel peptide recognition mode revealed by the X-ray structure of a core U2AF35/U2AF65 heterodimer. *Cell* 106(5):595–605.
14. Corsini L, et al. (2007) U2AF-homology motif interactions are required for alternative splicing regulation by SPF45. *Nat Struct Mol Biol* 14(7):620–629.
15. Zuo P, Maniatis T (1996) The splicing factor U2AF35 mediates critical protein-protein interactions in constitutive and enhancer-dependent splicing. *Genes Dev* 10(11):1356–1368.
16. Rudner DZ, Kanaar R, Breger KS, Rio DC (1998) Interaction between subunits of heterodimeric splicing factor U2AF is essential in vivo. *Mol Cell Biol* 18(4):1765–1773.
17. Wu S, Romfo CM, Nilsen TW, Green MR (1999) Functional recognition of the 3′ splice site AG by the splicing factor U2AF35. *Nature* 402(6763):832–835.
18. Zorio DA, Blumenthal T (1999) U2AF35 is encoded by an essential gene clustered in an operon with RRM/cyclophilin in Caenorhabditis elegans. *RNA* 5(4):487–494.
19. Merendino L, Guth S, Bilbao D, Martínez C, Valcárcel J (1999) Inhibition of msl-2 splicing by Sex-lethal reveals interaction between U2AF35 and the 3′ splice site AG. *Nature* 402(6763):838–841.
20. Yoshida H, et al. (2015) A novel 3′ splice site recognition by the two zinc fingers in the U2AF small subunit. *Genes Dev* 29(15):1649–1660.
21. Johnson JM, et al. (2003) Genome-wide survey of human alternative pre-mRNA splicing with exon junction microarrays. *Science* 302(5653):2141–2144.
22. Coolidge CJ, Seely RJ, Patton JG (1997) Functional analysis of the polypyrimidine tract in pre-mRNA splicing. *Nucleic Acids Res* 25(4):888–896.
23. Guth S, Martínez C, Gaur RK, Valcárcel J (1999) Evidence for substrate-specific requirement of the splicing factor U2AF(35) and for its function after polypyrimidine tract recognition by U2AF(65). *Mol Cell Biol* 19(12):8263–8271.
24. Banerjee H, et al. (2004) The conserved RNA recognition motif 3 of U2 snRNA auxiliary factor (U2AF 65) is essential in vivo but dispensable for activity in vitro. *RNA* 10(2):240–253.
25. Pacheco TR, Coelho MB, Desterro JM, Mollet I, Carmo-Fonseca M (2006) In vivo requirement of the small subunit of U2AF for recognition of a weak 3′ splice site. *Mol Cell Biol* 26(21):8183–8190.
26. Wang ET, et al. (2008) Alternative isoform regulation in human tissue transcriptomes. *Nature* 456(7221):470–476.
27. Kim E, Magen A, Ast G (2007) Different levels of alternative splicing among eukaryotes. *Nucleic Acids Res* 35(1):125–131.
28. Mackereth CD, et al. (2011) Multi-domain conformational selection underlies pre-mRNA splicing regulation by U2AF. *Nature* 475(7356):408–411.
29. Huang JR, et al. (2014) Transient electrostatic interactions dominate the conformational equilibrium sampled by multidomain splicing factor U2AF65: A combined NMR and SAXS study. *J Am Chem Soc* 136(19):7068–7076.
30. Sickmier EA, et al. (2006) Structural basis for polypyrimidine tract recognition by the essential pre-mRNA splicing factor U2AF65. *Mol Cell* 23(1):49–59.
31. Müller BK, Zaychikov E, Bräuchle C, Lamb DC (2005) Pulsed interleaved excitation. *Biophys J* 89(5):3508–3522.
32. Kudryavtsev V, et al. (2012) Combining MFD and PIE for accurate single-pair Förster resonance energy transfer measurements. *ChemPhysChem* 13(4):1060–1078.
33. Lee NK, et al. (2005) Accurate FRET measurements within single diffusing biomolecules using alternating-laser excitation. *Biophys J* 88(4):2939–2953.
34. Kapanidis AN, et al. (2004) Fluorescence-aided molecule sorting: Analysis of structure and interactions by alternating-laser excitation of single molecules. *Proc Natl Acad Sci USA* 101(24):8936–8941.
35. Kalinin S, Valeri A, Antonik M, Felekyan S, Seidel CAM (2010) Detection of structural dynamics by FRET: A photon distribution and fluorescence lifetime analysis of systems with multiple states. *J Phys Chem B* 114(23):7983–7995.
36. Antonik M, Felekyan S, Gaiduk A, Seidel CA (2006) Separating structural heterogeneities from stochastic variations in fluorescence resonance energy transfer distributions via photon distribution analysis. *J Phys Chem B* 110(13):6970–6978.
37. Soares LM, Zanier K, Mackereth C, Sattler M, Valcárcel J (2006) Intron removal requires proofreading of U2AF/3′ splice site recognition by DEK. *Science* 312(5782):1961–1965.
38. Agrawal AA, et al. (2016) An extended U2AF(65)-RNA-binding domain recognizes the 3′ splice site signal. *Nat Commun* 7:10950.
39. Yoshida K, et al. (2011) Frequent pathway mutations of splicing machinery in myelodysplasia. *Nature* 478(7367):64–69.
40. Senapathy P, Shapiro MB, Harris NL (1990) Splice junctions, branch point sites, and exons: sequence statistics, identification, and applications to genome project. *Methods Enzymol* 183:252–278.
41. Kanaar R, Roche SE, Beall EL, Green MR, Rio DC (1993) The conserved pre-mRNA splicing factor U2AF from Drosophila: Requirement for viability. *Science* 262(5133):569–573.
42. Rudner DZ, Kanaar R, Breger KS, Rio DC (1996) Mutations in the small subunit of the Drosophila U2AF splicing factor cause lethality and developmental defects. *Proc Natl Acad Sci USA* 93(19):10333–10337.
43. Mackereth CD, Simon B, Sattler M (2005) Extending the size of protein-RNA complexes studied by nuclear magnetic resonance spectroscopy. *ChemBioChem* 6(9):1578–1584.
44. Zhang Y, et al. (2013) Structure, phosphorylation and U2AF65 binding of the N-terminal domain of splicing factor 1 during 3′-splice site recognition. *Nucleic Acids Res* 41(2):1343–1354.
45. Tavanez JP, Madl T, Kooshapur H, Sattler M, Valcárcel J (2012) hnRNP A1 proofreads 3′ splice site recognition by U2AF. *Mol Cell* 45(3):314–329.
46. Manceau V, et al. (2006) Major phosphorylation of SF1 on adjacent Ser-Pro motifs enhances interaction with U2AF65. *FEBS J* 273(3):577–587.
47. Wang W, et al. (2013) Structure of phosphorylated SF1 bound to $U2AF^{65}$ in an essential splicing factor complex. *Structure* 21(2):197–208.
48. Eggeling C, et al. (2001) Data registration and selective single-molecule analysis using multi-parameter fluorescence detection. *J Biotechnol* 86(3):163–180.
49. Nir E, et al. (2006) Shot-noise limited single-molecule FRET histograms: comparison between theory and experiments. *J Phys Chem B* 110(44):22103–22124.
50. Schaffer J, et al. (1999) Identification of single molecules in aqueous solution by time-resolved fluorescence anisotropy. *J Phys Chem A* 103(3):331–336.
51. Gansen A, et al. (2009) Nucleosome disassembly intermediates characterized by single-molecule FRET. *Proc Natl Acad Sci USA* 106(36):15308–15313.
52. Schluesche P, Stelzer G, Piaia E, Lamb DC, Meisterernst M (2007) NC2 mobilizes TBP on core promoter TATA boxes. *Nat Struct Mol Biol* 14(12):1196–1201.
53. Sikor M, Mapa K, von Voithenberg LV, Mokranjac D, Lamb DC (2013) Real-time observation of the conformational dynamics of mitochondrial Hsp70 by spFRET. *EMBO J* 32(11):1639–1649.
54. Johnson BA, Blevins RA (1994) NMRView: A computer program for the visualization and analysis of NMR data. *J Biomol NMR* 4(5):603–614.
55. Battiste JL, Wagner G (2000) Utilization of site-directed spin labeling and high-resolution heteronuclear nuclear magnetic resonance for global fold determination of large proteins with limited nuclear overhauser effect data. *Biochemistry* 39(18):5355–5365.
56. Simon B, Madl T, Mackereth CD, Nilges M, Sattler M (2010) An efficient protocol for NMR-spectroscopy-based structure determination of protein complexes in solution. *Angew Chem Int Ed Engl* 49(11):1967–1970.